Z. angew. Math. Phys. 54 (2003) 1050–1072
0044-2275/03/061050-23
DOI 10.1007/s00033-003-1108-x

Zeitschrift für angewandte Mathematik und Physik ZAMP

Numerical investigation of the Liebau phenomenon

Alfio Borzì and Georg Propst

Abstract. The Liebau phenomenon is the occurrence of valveless pumping through the application of a periodic force at a place which lies asymmetric with respect to system configuration. This paper is concerned with two different physical configurations and respective models. Comparison and derivation among the models is discussed. Accurate numerical schemes which solve these models are presented. By means of numerical simulations it is investigated under which conditions valveless pumping takes place.

Mathematics Subject Classification (2000). 76B15, 92C35, 35L45, 35L50, 65M99.

Keywords. Valveless pumping.

1. Introduction

In 1954, Gerhart Liebau published a short article [7] where he observed that the amount of energy associated to blood circulation might not be explainable solely by the work exercised by the heart. He made the suggestion that a regular oscillatory compression of at least part of the cardiovascular system, for example through the respiratory movements, together with asymmetry of the cardiovascular system with respect to the place where compression takes place could explain the high efficiency with which blood circulation occurs. To sustain his hypothesis he made concrete experiments using elastic tubes with different lengths and different elastic properties and showed the occurrence of a valveless pumping effect. We refer to this as the Liebau phenomenon.

A first attempt to model the Liebau phenomenon is due to von Bredow [2] who derived a set of linear equations obtained from the Navier-Stokes equations with some simplifying assumptions. The system configuration he considered is depicted in Fig. 1. Later, Rath and Teipel [10] considered a nonlinear model for an elastic tube connecting two tanks filled with water. In both papers there were indications that the Liebau phenomenon could also occur using rigid pipes. In fact, in 1985 Takagi and Takahashi [11] proposed a model for rigid pipes and could show the occurrence of valveless pumping in real experiments and numerical simulations. More recently a two-dimensional simulation of an annular system of two pieces of

elastic tubes that have different elasticity properties has been considered [3]. Also in this case the application of a periodic force which acts asymmetrically gives rise to net flow.

The models proposed in [2, 10, 11] never received much attention probably because there was no real need for valveless pumps which are in general less efficient than pumps with valves. However, there is nowadays renewed interest in valveless pumping. Recent results in physiology [8] indicate that highest efficiency of pumping in cardiovascular systems is reached through cooperation of heart pumping with valves and valveless pumping through respiration. There is also the observation [8] that some invertebrates possess a valveless circulatory system which again motivates a better understanding of this phenomenon. Valveless pumps have been proposed recently [1] based on special diffuser configurations. Another example of a valveless pump is given in [9] where a lunar-shaped polyurethane-made blood chamber with an oscillating disk is used for pumping. However, to the best of our knowledge there are no examples of use of the Liebau phenomenon for technological applications and it is one of the purpose of the present paper to support such applications. Also recently, intensive research has been focused on the development of micro- and nanosystems. As in [11] one could make use of the pumping effect in rigid systems to design pumps for micro machines using silicon-glass stack [1]. Another challenging attempt would be to construct pumps using nanotubes [12].

In this paper we consider two-tanks configurations (as opposed to annular systems), in particular we investigate the models considered in [2, 10, 11]. Despite differences among them, the Liebau phenomenon can be observed with all these models. In the next section we present the numerical solution of the model for elastic tubes. The numerical algorithm is described in detail and results of simulations are presented. In [10] it is argued that the nonlinearity in the model is responsible for the valveless pumping effect. In this paper we show that this is not the case. In fact, linearizing the nonlinear model we obtain the linear model considered in [2] and show, via numerical experiments, the occurrence of the Liebau phenomenon also in the linear case. See Section 3.2 and Section 4. While [2, 10] consider infinite dimensional systems, in [11] a system of ordinary differential equations is investigated. This model was written for a physical configuration similar to that depicted in Fig. 1 but using closed tanks, rigid pipes, and a 'rigid' forcing system. For this reason a direct comparison of the results presented in [11] with those shown in [2, 10] is not possible. We therefore consider modifications of the configuration in [11] and change the model correspondingly. In Section 5 the model proposed in [11] and those that we derived from it are investigated numerically and the results obtained from these models are compared with those obtained with the models for elastic tubes.

Of course it is desireable to develop a theory that explains valveless pumping from basic principles. Such a theory is not contained in the present article. Nevertheless, we believe that systematic modeling and comparative simulations are

valuable contributions towards the understanding of the Liebau phenomenon.

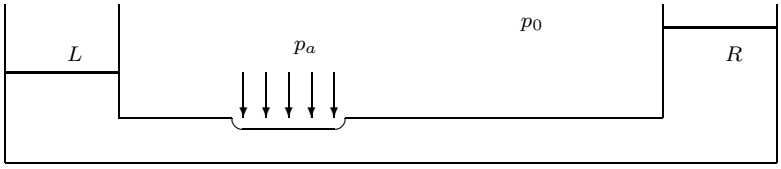

Figure 1. A Liebau pump.

2. A model for elastic tubes

This section is concerned with the pumping effect without valves in a system with an elastic tube which connects two open tanks; see Fig. 1. At the beginning the two tanks and the tube are filled with an incompressible fluid (e.g. water) of density ρ, at rest. By acting with a periodic external force on a region of the pipe situated asymmetrically with respect to the two tanks, a net flow occurs which results in a pumping of fluid into one tank at the cost of the other tank. Once reached, this pressure difference is maintained.

This system was solved numerically in [10]. The numerical method used was the MacCormack scheme and the boundary conditions remained unclear. In this paper we present the implementation of a modern Godunov scheme and provide a detailed description of the boundary conditions and of their numerical treatment. We then investigate the importance of various components in the model in order to identify the essential pre-requisite to obtain a valveless pumping effect.

Consider an elastic tube of length L and cross section area $A_0 = \pi D_0^2/4$ (at rest) attached to two tanks of cross section area A_B (B for Behälter, German for tanks). The origin of the coordinate system is placed at the attachment of the tube with the left-hand tank, the positive x axis pointing to the right. In the region $x_L \le x \le x_R$ we assume an oscillatory pressure acting on the walls of the elastic tube given by:

$$p_a(x,t) = p_0 + 2\,p_0 \frac{(x-x_L)(x_R-x)}{(x_R-x_L)^2}\,\sin\omega t, \tag{1}$$

where p_0 is the constant ambient pressure and ω is the angular frequency of the periodic acting force. For $x \notin [x_L, x_R]$ we have $p_a(x,t) = p_0$.

The equations that describe the fluid flow inside the pipe are, as in [10],

$$\frac{\partial w}{\partial t} + w\frac{\partial w}{\partial x} + \frac{1}{\rho}\frac{\partial p}{\partial x} = -\frac{1}{\rho}\frac{\partial p_\nu}{\partial x}, \tag{2}$$

$$\frac{\partial p}{\partial t} + w\frac{\partial p}{\partial x} + \rho a^2\frac{\partial w}{\partial x} = \frac{\partial p_a}{\partial t} + w\frac{\partial p_a}{\partial x}, \tag{3}$$

where $w(x,t)$ is the flow velocity and $p(t,x)$ is the total pressure. Here, the right-hand side term of the momentum equation (2) represents the viscosity in the laminar approximation given by Hagen–Poiseuille:

$$\frac{\partial p_\nu}{\partial x} = 8\pi\mu\frac{w}{A_0}, \tag{4}$$

where μ is the viscosity coefficient. The continuity equation (3), in terms of pressure, is derived using the equation of state $A = A_0\left[1 + \frac{D_0}{2s}\frac{p-p_a}{E}\right]^2$ relating $p(x,t)$ and $A(x,t)$, the cross section of the tube at (x,t). The right-hand side of (3) describes the forcing term. The factor a^2 in (3) represents the velocity of travelling waves and is given by

$$a^2 = a_0^2\left[1 + \frac{D_0}{2s}\frac{p-p_a}{E}\right], \tag{5}$$

where $a_0 = \sqrt{\frac{sE}{\rho D_0}}$, s is the thickness of the pipe wall, and E is the Young modulus.

The hyperbolic system (2)–(3) can be re-written as

$$\frac{\partial}{\partial t}\begin{pmatrix} w \\ p \end{pmatrix} + \begin{bmatrix} w & \frac{1}{\rho} \\ \rho a^2 & w \end{bmatrix}\frac{\partial}{\partial x}\begin{pmatrix} w \\ p \end{pmatrix} = \begin{pmatrix} F \\ G \end{pmatrix}, \tag{6}$$

where $F = -8\pi\mu\frac{w}{\rho A}$ and $G = \frac{\partial p_a}{\partial t} + w\frac{\partial p_a}{\partial x}$; we set $\Gamma = \begin{pmatrix} F \\ G \end{pmatrix}$.

In the following, we denote with $q = \begin{pmatrix} w \\ p \end{pmatrix}$ the state vector of primitive variables w and p and define the matrix

$$C(q) = \begin{bmatrix} w & \frac{1}{\rho} \\ \rho a^2 & w \end{bmatrix}. \tag{7}$$

This matrix is diagonalized through the transformation

$$Q_C^{-1}C(q)Q_C = \Lambda = diag\{w+a, w-a\}, \tag{8}$$

where Q_C and Q_C^{-1} are given by

$$Q_C = \begin{bmatrix} \frac{1}{2} & \frac{1}{2} \\ \frac{\rho a}{2} & -\frac{\rho a}{2} \end{bmatrix} \text{ and } Q_C^{-1} = \begin{bmatrix} 1 & \frac{1}{\rho a} \\ 1 & -\frac{1}{\rho a} \end{bmatrix}. \tag{9}$$

Therefore the problem (6) can be given a characteristic form by multiplying it from the left with Q_C^{-1} and introducing characteristic variables v such that $\delta v =$

$Q_C^{-1}\delta q$. In other words, (6) can be expressed in the form

$$d_+ w + \frac{1}{\rho a} d_+ p = (Q_C^{-1}\Gamma)_1 \text{ and } d_- w - \frac{1}{\rho a} d_- p = (Q_C^{-1}\Gamma)_2, \tag{10}$$

where $d_\pm \phi = \frac{\partial \phi}{\partial t} + (w \pm a)\frac{\partial \phi}{\partial x}$.

Regarding the boundary conditions at $x = 0$, we have

$$\begin{cases} p(t,0) &= p_B^L(t) - \frac{1}{2}\,\rho\, w(t,0)^2 \,\left(\frac{1+\text{sign}\, w(t,0)}{2}\right), \\ A(t,0) &= A_0, \\ \frac{d}{dt} p_B^L(t) &= -\rho g(\frac{A_0}{A_B})\, w(t,0), \end{cases} \tag{11}$$

with given initial condition $p_B^L(0)$ on the pressure of the left-hand tank. At the right-hand boundary, $x = L$, we have

$$\begin{cases} p(t,L) &= p_B^R(t) - \frac{1}{2}\,\rho\, w(t,L)^2 \,\left(\frac{1-\text{sign}\, w(t,L)}{2}\right), \\ A(t,L) &= A_0, \\ \frac{d}{dt} p_B^R(t) &= \rho g(\frac{A_0}{A_B})\, w(t,L), \end{cases} \tag{12}$$

with given initial condition $p_B^R(0)$ on the pressure of the right-hand tank. p_B^L and p_B^R are state components of the model.

3. Numerical solution of the elastic tube problem

We present a numerical algorithm that solves equations (2)-(3) with the given boundary conditions (11)–(12). We solve the present problem by using a second-order MUSCL-Hancock scheme in non-conservative form with a primitive variable Riemann Solver (PVRS); see [13] for the details.

For the purpose of presentation, it is convenient to write equation (6) in the form

$$\frac{\partial}{\partial t} q + C(q)\frac{\partial}{\partial x} q = \Gamma(x,q). \tag{13}$$

In the following, $[0, L]$ is the spatial domain. The boundary conditions are assumed to be represented by the boundary functions $q_1(t)$ and $q_2(t)$. The initial condition is given by $q^0(x)$ at time $t = 0$. Assume that the spatial domain $[0, L]$ has been discretized in a finite number N_{cell} of cells of uniform mesh size Δx indexed by i.

In the present approach, the discrete state vector function q_i^n denotes the cell average of the state vector variable $q(x,t)$ in the cell with index i at the time level n, $t = t^n = n\Delta t$. With such averages a piecewise constant vector function $q(x)$ is defined with value q_i^n in the i-th cell and jump discontinuities at each cell interface $x_{i+1/2}$, $i = 1, 2, \ldots N_{cell} - 1$. On the cell edge $x_{i+1/2}$ we denote with $q_{i+1/2}^L$ and $q_{i+1/2}^R$ the left- and right-hand side vector values of $q(x)$ at the edge.

The MUSCL-Hancock scheme to solve (13) is formally given by

$$q_i^{n+1} = q_i^n + \frac{\Delta t}{\Delta x} C_i(\bar{q}_i)[q_{i-1/2}^{n+1/2} - q_{i+1/2}^{n+1/2}] + \Gamma(x_i, \bar{q}_i), \tag{14}$$

where the matrix $C_i(\bar{q}_i)$ is defined at the grid point i and $\bar{q}_i = (q_{i-1/2}^n + q_{i+1/2}^n)/2$. The intermediate states $q_{i\pm1/2}^{n+1/2}$ are defined at the intermediate positions $i \pm 1/2$ at the half-time level $n + 1/2$. Notice that (14) is centered in time and space.

To describe the entire algorithm let us first assume that the solution at the time level n has been computed. In order to compute the solution at the next time level the following steps are due:

Step (I) Reconstruction.

The data cell average values q_i^n are locally replaced by piecewise linear functions in each cell $I_i = [x_{i-1/2}, x_{i+1/2}]$, namely

$$q(x) = q_i^n + (x - x_i)\,\sigma_i, \quad x \in I_i, \tag{15}$$

where σ_i is a suitable second-order accurate non-oscillatory slope. We use the ENO scheme [5, 6] for this purpose.

Step (II) Extrapolation.

At the cell edge $x_{i+1/2}$ we obtain (including tube ends)

$$q_{i+1/2}^L = q_i + \frac{\Delta x}{2}\sigma_i \text{ and } q_{i+1/2}^R = q_{i+1} - \frac{\Delta x}{2}\sigma_{i+1}. \tag{16}$$

Step (III) Evolution.

We evolve the values $q_{i+1/2}^L$ and $q_{i+1/2}^R$ by a half-time step using (including tube's ends)

$$\tilde{q}_{i\pm1/2}^{L,R} = q_{i\pm1/2}^{L,R} + \frac{1}{2}\frac{\Delta t}{\Delta x} C_i(q_i^n)[q_{i-1/2}^L - q_{i+1/2}^R] + \Gamma(x_i, q_i^n), \tag{17}$$

Step (IV) The Approximate Riemann Solver.

The data defined in Step (III) is used to set up a Riemann problem on each cell edge at $x_{i+1/2}$ with piecewise constant initial data $(q_{i+1/2}^L, q_{i+1/2}^R)$:

$$\begin{aligned} \frac{\partial}{\partial t} q + C(q)\frac{\partial}{\partial x} q &= 0, \\ q(x,0) &= q_L, \quad x < x_{i+1/2}, \\ q(x,0) &= q_R, \quad x > x_{i+1/2}. \end{aligned} \tag{18}$$

Here, the domain of interest is the $x-t$ plane with $t > 0$ and $-\infty < x < \infty$. In practice, for our purpose, x varies in a finite interval, say $[x_i, x_{i+1}]$. The solutions of two contiguous Riemann problems will not interact if the CFL condition is satisfied; see, e.g., [4]. Therefore, under this condition a unique solution $q^*(0, q_L^n, q_R^n)$ (or simply q^*) to the Riemann problem can be found at the interface for the time $t \in [t^n, t^{n+1}]$ and we set

$$q_{i+1/2}^{n+1/2} = q^*(0, q_L^n, q_R^n)_{i+1/2}. \tag{19}$$

A way of obtaining approximate solutions to (18) is to use the characteristic equations (10) with zero right-hand sides. It follows that considering the right-going characteristic, $dx/dt = w + a$, traversing the interface at $x_{i+1/2}$, we have

$$(p^* - p^L)/\rho + \bar{a}\,(w^* - w^L) = 0, \tag{20}$$

where $(w^*, p^*) = q^*(0, q_L^n, q_R^n)$ is the solution sought and $\bar{a} = (a^L + a^R)/2$. In the same way, considering the left-going characteristic, $dx/dt = w - a$, traversing the same interface, we obtain

$$(p^R - p^*)/\rho - \bar{a}(w^R - w^*) = 0. \tag{21}$$

The complete solution is then given by

$$p^* = \frac{1}{2}(p^L + p^R) + \frac{1}{2}(w^L - w^R)(\rho\bar{a}), \tag{22}$$

$$w^* = \frac{1}{2}(w^L + w^R) + \frac{1}{2}(p^L - p^R)\frac{1}{\rho\bar{a}}. \tag{23}$$

This solution can safely be used if the following conditions are met [13]:

$$\frac{p_{max}}{p_{min}} < c,$$

where $c = O(1)$, and $p_{max} = \max(p^L, p^R)$ and $p_{min} = \min(p^L, p^R)$. The other condition is $p_{min} < p^* < p_{max}$.

Notice that at the left-hand tube end we only have q^R and at the right-hand tube end we only have q^L. Therefore, in order to solve the Riemann problem at the tube ends, additional conditions must be supplied. This problem is solved in the next section devoted to boundary conditions treatment.

Assuming that we have q^*, that is $q^{n+1/2}$ at the cell edges, we can apply (14) to compute the solution for the next time level. So we have completed the description of the algorithm to solve the interior tube problem.

3.1. Boundary conditions treatment

Consider the left-hand tube end. At $x = 0$ the left going characteristic points towards the left-hand tank and is described by

$$(p^R - p^*)/\rho - \bar{a}(w^R - w^*) = 0,$$

where w^* and p^* are the unknown solution values of flow velocity and pressure at the attachment. To solve for these variables, we first look for no-flow conditions which are characterized by $w^* = 0$. In correspondence we have

$$p^*_{ref} = p^R - \rho\,\bar{a}\,w^R. \tag{24}$$

Here p^*_{ref} represents the pressure for which no-flow occurs. In a similar way we find the reference pressure for the right-hand tube end

$$p^*_{ref} = p^L + \rho\,\bar{a}\,w^L. \tag{25}$$

Having the reference pressure at disposal, flow into the tank occurs if $p^*_{ref} > p_B$, where p_B denotes the static pressure in the tank (at the attachment level). In the other case, $p^*_{ref} < p_B$, the fluid will leave the tank and enter the tube. Let us denote by p^L_B and by p^R_B the pressure in the left-hand and right-hand tanks, respectively.

Consider again the left-hand tube end. If $p^*_{ref} > p^L_B$, flow from the tube into the tank occurs. We assume quasi-steady flow across the boundary. Quasi steady means that it is assumed that the flow across the boundary behaves at each instant of time as a steady flow under the same conditions. This means, for example, that the time a pressure wave needs to travel across the tube cross section at the boundary is much smaller than the time scale with which the conditions change. Under this assumption, the boundary problem at the left-hand tube end is defined by

$$\left\{\begin{array}{lcl} p^* & = & p^L_B, \\ w^* & = & w^R + (p^* - p^R)\frac{1}{\rho\bar{a}}, \\ \frac{d}{dt}p^L_B & = & \rho g(\frac{A_0}{A_B})(-w^*). \end{array}\right. \tag{26}$$

where g is the gravity constant. The last equation of (26) corresponds to the continuity equation $A_B\, w_B = A_0\, w^*$ between tank and tube. The solution of this boundary problem is obtained substituting the first equation and the second equation of (26) in the third equation and integrating the resulting ODE with initial condition $p^*(0) = p^L_B(0)$ for half-time step. Here $p^L_B(0)$ denotes the pressure of the tank from previous time step. We obtain

$$p^* = p^*_{ref} + (p^L_B(0) - p^*_{ref})e^{-\frac{g}{\bar{a}}(\frac{A_0}{A_B})\frac{\Delta t}{2}}. \tag{27}$$

Correspondingly, the solution of the boundary problem at the right-hand tube end is given by

$$p^* = p^*_{ref} + (p^R_B(0) - p^*_{ref})e^{-\frac{g}{\bar{a}}(\frac{A_0}{A_B})\frac{\Delta t}{2}}. \tag{28}$$

The velocity w^* then follows from (20) for the right-hand tube end and from (21) for the left-hand tube end, respectively. The new pressure values for the tanks are then obtained by

$$p^L_B = p^L_B + \rho g(\frac{A_0}{A_B})(-w^*)\Delta t \quad \text{and} \quad p^R_B = p^R_B + \rho g(\frac{A_0}{A_B})(w^*)\Delta t \tag{29}$$

In case of $p^*_{ref} < p^L_B$, flow from the tank into the tube occurs. Under quasi-steady conditions, the boundary problem at the left-hand tube end is now

$$\left\{\begin{array}{lcl} p^* & = & p^L_B - \frac{1}{2}\rho(w^*)^2, \\ w^* & = & w^R + (p^* - p^R)\frac{1}{\rho\bar{a}}, \\ \frac{dp^L_B}{dt} & = & \rho g(\frac{A_0}{A_B})(-w^*). \end{array}\right. \tag{30}$$

Substituting the first equation of (30) in the second one and solving for $(w^*/\bar{a})$

we obtain

$$(\frac{w^*}{\bar{a}}) = -1 + \sqrt{1 + 2(\frac{w^R}{\bar{a}}) + 2\frac{(p_B^L - p^R)}{\rho\bar{a}^2}}. \tag{31}$$

This solution is then substituted in the third equation of (30) to obtain p_B^L as a solution of the differential equation

$$\frac{dp_B^L}{dt} = \rho g(\frac{A_0}{A_B})\bar{a}\left[1 - \sqrt{1 + 2(\frac{w^R}{\bar{a}}) + 2\frac{(p_B^L - p^R)}{\rho\bar{a}^2}}\right].$$

Therefore the approximate value of p_B^L at half-time step is given by

$$p_B^L(\Delta t/2) = p_B^L(0) + \frac{\Delta t}{2}\rho g(\frac{A_0}{A_B})\bar{a}\left[1 - \sqrt{1 + 2(\frac{w^R}{\bar{a}}) + 2\frac{(p_B^L(0) - p^R)}{\rho\bar{a}^2}}\right].$$

This value is inserted in (31) to obtain w^*. The new value of the pressure at the tube end follows

$$p^* = p_B^L - \frac{1}{2}\rho(w^*)^2. \tag{32}$$

With the same reasoning we obtain the solution at the right-hand tube end, using

$$(\frac{w^*}{\bar{a}}) = -1 - \sqrt{1 - 2(\frac{w^L}{\bar{a}}) + 2\frac{(p_B^R - p^R)}{\rho\bar{a}^2}}, \tag{33}$$

and

$$p^* = p_B^R - \frac{1}{2}\rho(w^*)^2. \tag{34}$$

Once the new values of w^* are obtained, equations (29) provide the pressure in the tanks for the next time step.

The values of w^* and of p^* for the half-time step at the tube ends are used in equation (14), to advance in time. The equations (29) are used to update the pressure in each tank for the next time step.

3.2. Linearization of the elastic tube model

Consider the system (2)–(3) in the case of small disturbances where $A = A_0 + A'$, $p = p_0 + p'$, and $w = w'$. Neglecting second-order terms, we obtain

$$\frac{\partial w'}{\partial t} + \frac{1}{\rho}\frac{\partial p'}{\partial x} = -\frac{1}{\rho}\frac{\partial p_\nu}{\partial x} =: F, \tag{35}$$

$$\frac{\partial p'}{\partial t} + \rho a_0^2\frac{\partial w'}{\partial x} = \frac{\partial p_a}{\partial t} + w'\frac{\partial p_a}{\partial x} =: G. \tag{36}$$

This system can be put in the form (6) where w is set to zero in the main diagonal of C. Notice that the characteristic equations remain unchanged under the linearization process.

If we perform the same type of linearization for the boundary problem, that is, neglect the quadratic terms, we obtain (26) for the inflow and outflow problems. Therefore the solution is given by (27) and (28) for both inflow and outflow. The velocity at the tube ends is obtained using the characteristic equations (20) and (21).

By differentiation and a little algebra, equations (35)-(36) can be put in form of the wave equation, namely

$$\frac{\partial^2 w'}{\partial t^2} - a_0^2 \frac{\partial^2 w'}{\partial x^2} = \frac{\partial F}{\partial t} - \frac{1}{\rho}\frac{\partial G}{\partial x}, \tag{37}$$

$$\frac{\partial^2 p'}{\partial t^2} - a_0^2 \frac{\partial^2 p'}{\partial x^2} = \frac{\partial G}{\partial t} - \rho a_0^2 \frac{\partial F}{\partial x}, \tag{38}$$

In particular, consider equation (37) in the region of the tube without external forcing action, $G = 0$. In this case and using (4), equation (37) becomes

$$\frac{\partial^2 w'}{\partial t^2} - a_0^2 \frac{\partial^2 w'}{\partial x^2} + \left(\frac{8\pi\mu}{\rho A_0}\right) \frac{\partial w'}{\partial t} = 0. \tag{39}$$

Equation (39) represents the model suggested in [2]. However, in [2] the differential operator in (39) applies to the variable $Q(t, x)$ defined as 'volume' such that $\partial Q/\partial t = w'$. Taking this fact into account the boundary conditions for (39) can be formulated, as in [2], as follows

$$-a_0^2 \frac{\partial w'}{\partial x} = g\left(\frac{A_0}{A_B}\right)(-w') \text{ at the left-hand tube end.} \tag{40}$$

These boundary conditions can be obtained combining equation (5) with (37)–(38) and the third equation in (11).

It is interesting to notice that in [2] much effort is invested to demonstrate that a linear model like (39) exhibits the Liebau phenomenon. On the other hand in [10] it is stated that valveless pumping can only be explained in terms of a nonlinear model. In this section we have shown the relation between the two models and in the next section we demonstrate that both the nonlinear system and the linear system are able to model valveless pumping.

4. Numerical experiments with the elastic tube model

We investigate the contribution of various terms in the model (2)–(3), (11)–(12) in order to find a minimum set of conditions under which a valveless pumping effect can be observed. In the following experiments we always use $N_{cell} = 100$ and $\Delta t = (0.1/a_0)\Delta x$.

For comparison we consider the setting given in [10]. That is (in CGS) $L = 180$ cm, $\rho = 0.998$ g/cm^3, $\mu = 9 \cdot 10^{-3}$ g/cms and $a_0 = 11.95 \cdot 10^2$ cm/s. Further we have $x_L/L = 0.2$ and $x_R/L = 0.4$ and $\omega = 14.6$ $1/s$. We assume two equal tanks with various cross sections $A_B = n_A A_0$ with $n_A = 25, 50, 75, 100$,

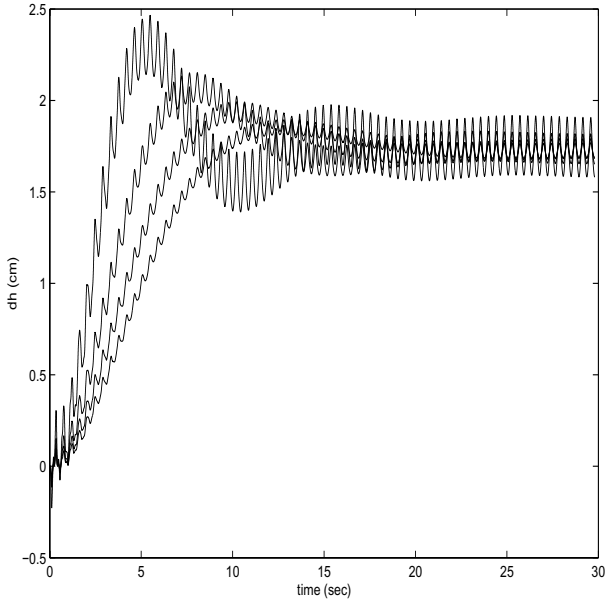

Figure 2. Development of level differences with time for $n_A = 25, 50, 75, 100$. At the beginning dh increase faster for smaller n_A. Here $\mu = 0$ and $a = a_0$.

and $A_0 = \pi D_0^2/4$ where $D_0 = 5\ \ cm$. Corresponding to this setting we plot in Fig. 2 the evolution history of the level difference between the two tanks given by $dh = (p_B^R - p_B^L)/(\rho g)$. In the figure we can observe that the amount of time required to reach an average steady state changes almost linearly with the change of the area of the cross section of the tanks as is to be expected when the delivery of the tube remains the same. Notice that the highly-oscillating part of the curves corresponds to the pulsating pressure p_a.

By performing experiments with various μ, including $\mu = 0$, we observe that in this case the pumping effect is not due to the presence of viscosity. For $\mu = 0$ the resulting pumping effect is qualitatively the same as that observed with non-zero viscosity. On the other hand increasing μ reduces the pumping efficiency of the system, that is, the difference of pressure between the tanks. Also the dependence of a on p as given by (5) is not essential to have valveless pumping. In numerical experiments we obtain results that show that even with $a = a_0$, a similar pumping effect is obtained.

In earlier experimental observations [7] the occurrence of valveless pumping was related to asymmetric configurations, whereas the asymmetry could have been due to different lengths of the two arms of the tube or equal length but different Young modulus or different cross sections. This fact seems to suggest that the Liebau phenomenon is related to the interaction between forced oscillation due to the periodic forcing term having frequency ω and the autowaves of the system

corresponding to eigenfrequency which are determined by the geometry and other physical properties of the system. Assuming a forced wave of frequency ω which propagates with speed a_0 along the tube, the corresponding wavelength is given by $\lambda = a_0 \frac{2\pi}{\omega}$. The geometry is then represented by the length of the tube L in units of λ and the physical properties enter all in the definition of the wave velocity a_0.

For these reasons we now focus our attention on the frequency ω and on the position where the forcing term is applied. Assume a given frequency, set $L = \lambda$ and consider a standing wave of the form $\cos(2\pi x/\lambda)$ superimposed on the tube. At the ends of the tube this function has value one, corresponding to the open tube ends and maximal flow velocity. Let us denote by $x_f = (x_L + x_R)/2$ the position at which the forcing term $p_a(x, \cdot)$ symmetrically applies. It is known [2, **?**] that independently of the length of the tube and of the excitation frequency no pumping effect occurs when the exciting function $p_a(x, \cdot)$ is centered at x_0, that is, halfway between the two tanks. On the other hand, the cosinus function considered above is symmetric with respect to x_0 and is zero at $x_f = k\lambda/4$, $k = 1, 3$. Therefore we performed experiments where the periodic forcing function was centered at these 'zero' points and no net pumping effect was observed. We can summarize the results of our experiments as follows.

Pumping effect depending on x_f, $L = \lambda$, and $\mu = 0$.

1. If $0 < x_f < \lambda/4$ or $\lambda/2 < x_f < 3\lambda/4$, pumping from right to left occurs.
2. If $\lambda/4 < x_f < \lambda/2$ or $3\lambda/4 < x_f < \lambda$, pumping from left to right occurs.

On the other hand we could expect that changes in ω will be equivalent to changes of x_f. In fact, reducing ω, with L held fixed, it happens that if the first node of $\cos(2\pi x/\lambda)$ is situated to the left of x_0, then, if $0 < x_f < x_0$, pumping from right to left occurs. In case when $x_0 < x_f < L$, pumping from left to right occurs. By further reducing ω below the value $\omega_0 = a_0\pi/L$ it happens that the opposite situation occurs. Therefore for a given L and x_f, increasing ω will eventually result in repeated inversions of the pumping direction. This occurrence has been observed in [2, 10]. For completeness we report the results of an experiment where flow inversion occurs. Consider the original setting with $\omega = 14.6$, $x_f = 0.3L$, $n_A = 50$, and $\mu = 0$. We report in Fig. 3 the results of experiments obtained with $\omega = 14.6$ and with $\omega = 29.2$, while $\omega_0 = 20.87$.

Let us now consider the linear model (37)–(38) with boundary conditions given by (11)-(12) without quadratic terms. In this case we find out that the viscosity μ plays an important role in the pumping effect. In fact, without viscosity, the difference of water levels oscillates with the frequency of the forcing function but with an amplitude which is much larger than the average net pumping. This result is shown in Fig. 4 (a), which has been obtained solving the linear model with $\mu = 0$ and using $L = 180$, $a_0 = 1195$, $x_L/L = 0.2$, $x_R/L = 0.4$, $n_A = 50$, and $\omega = 14.6$.

To have a pumping effect comparable with that of the nonlinear model with the same configuration a large value for μ must be chosen. For example, in Fig. 4

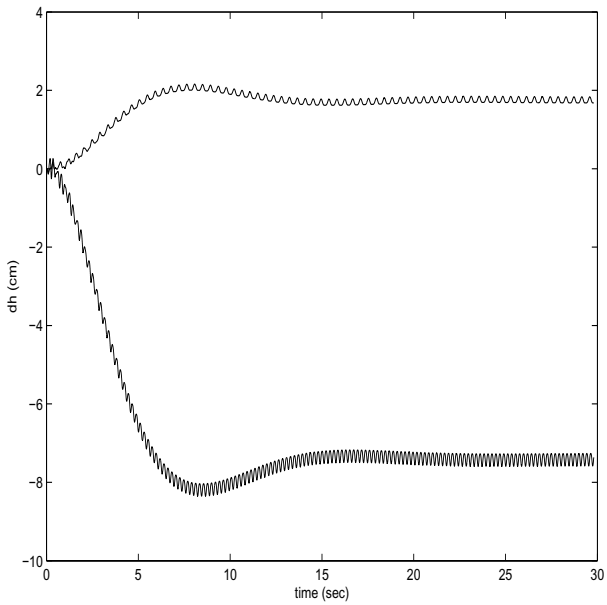

Figure 3. Development of (pressure) level difference with time for $\omega = 14.6$ (positive dh) and $\omega = 29.2$ (negative dh). Here $\mu = 0$ and $a = a_0$.

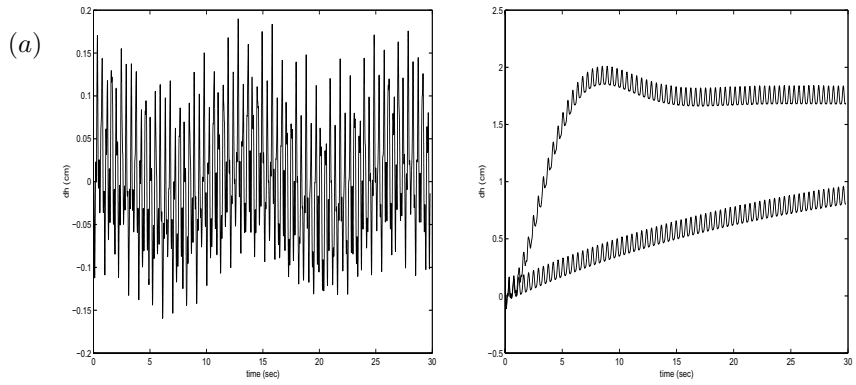

Figure 4. (a) Result from linear model with $\mu = 0$; (b) results from linear and nonlinear model.

(b), results obtained with the nonlinear model with $\mu = 0.09$ and with the linear model with $\mu = 0.09 \times 50$ are compared. The level difference grows in shorter time in the nonlinear model.

To show graphically the result stated above, the changes of the observed pumping efficiencies of the linear and the nonlinear model as x_f changes are reported in Fig. 5. In these pictures L is held constant and two frequencies are considered.

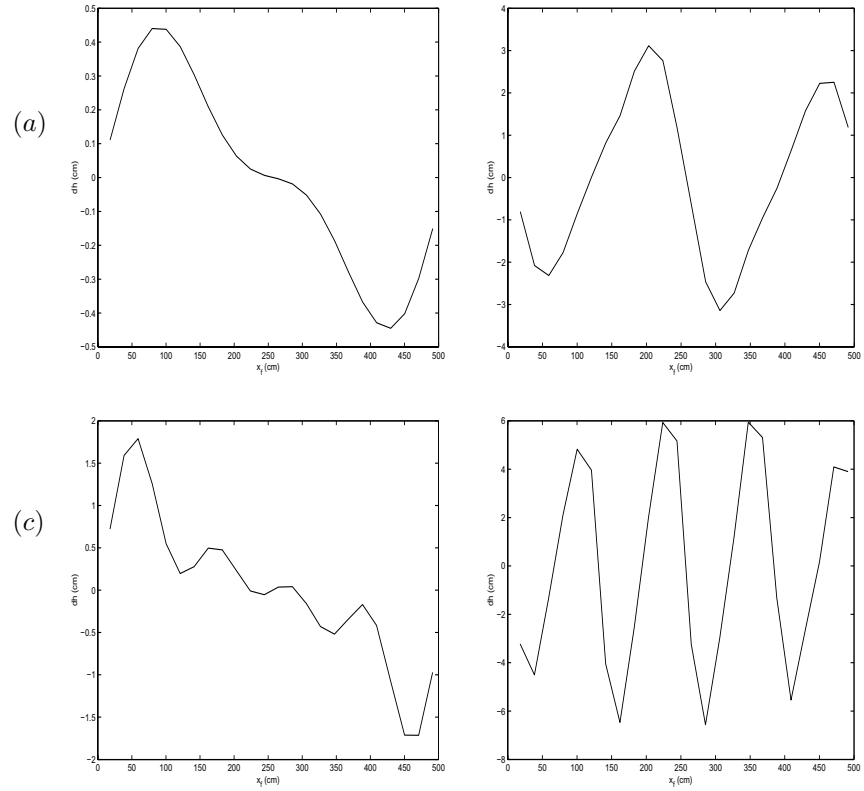

Figure 5. $L = \lambda(\omega_0)$, $\omega_0 = 14.6$: (a) Result from linear model with $\omega = \omega_0$; (b) results from nonlinear model with $\omega = \omega_0$; (c) Result from linear model with $\omega = 2\omega_0$; (d) results from nonlinear model with $\omega = 2\omega_0$.

In the linear case a different behavior is observed. Notice also that the pumping effect increase with ω .

5. Rigid pipes

In the configuration of [11], two tanks are connected to two inelastic rigid pipes of length ℓ_1 and ℓ_2 of constant cross-section A_0 . The pipes are connected by a three way tee, its third exit leading to a cylinder of cross-section A_c . This cylinder is closed by a piston at position $y(t)$ that is moved periodically, $y(t) = S_p \sin(\omega t + \delta)$. Another difference to the configurations in the previous sections is, that in [11] the tanks are closed and the air above the water in the tanks is pressurized (so that the eigenfrequency of the linearized system is adjustable).

The following models do not use the spatial coordinate x, instead, there are two indices for the two tanks and pipes. Let w_i denote the velocity of the incompressible fluid in pipe i, in direction from the tee toward the tank i. The conservation of mass in the tee reads

$$A_0(w_1(t) + w_2(t)) = A_c S_p \omega \cos(\omega t + \delta). \tag{41}$$

With $m_i = \rho \ell_i$, the momentum equations for the fluid in the pipes are

$$\frac{d}{dt} m_i w_i(t) = p_i^b(t) - p_i^e(t) - p_i^v(t), \quad i = 1, 2. \tag{42}$$

p_i^v stands for friction due to viscosity, that is modeled by Blasius' law for turbulent flow

$$p_i^v = 0.3164 \, \frac{\rho}{2} \frac{\ell_i}{D_0} \operatorname{sign} w_i \left(\frac{\mu}{D_0 \rho |w_i|} \right)^{1/4} w_i^2.$$

p_i^b are the pressures at the beginning of the pipes at the tee, and p_i^e are the pressures at the end of the pipes near the tanks. The latter ones are set to

$$p_i^e(t) = p^a(h_i(t)) + \rho g h_i(t) - \frac{1}{2}(1 - \operatorname{sign} w_i(t))(1 + \zeta) \frac{\rho}{2} w_i(t)^2. \tag{43}$$

$h_i(t)$ is the level height in tank i and ζ is a friction coefficient. Because of the signum, the pressure drop due to acceleration only applies for flow from the tank into the pipe. The terms $p^a(h) = q_0 + q_1 h$ with constants q_0, q_1 model pressure due to the compression of the air above the fluid in the closed tanks (for simplicity we consider identical configurations of the two tanks). The difference of the pressures at the tee is given by

$$p_1^b - p_2^b = \frac{\rho}{2}(w_2^2 - w_1^2) + \zeta_{12}(w_1, w_2) T(w_1, w_2)$$

where ζ_{12} and the function T incorporate the various possible flow patterns in the tee (see [11] and the references therein, the details are not needed here). With this we arrive at a system of equations for $w^- := m_1 w_1 - m_2 w_2$, h_1 and h_2 and a forcing function on $w^+ := w_1 + w_2$

$$\frac{d}{dt} w^- = p_1^b - p_2^b - p_1^e + p_2^e - p_1^v + p_2^v \tag{44}$$

$$\frac{d}{dt} h_i = \frac{A_0}{A_B} w_i, \quad i = 1, 2 \tag{45}$$

$$w^+(t) = \frac{A_c S_p \omega}{A_0} \cos(\omega t + \delta) \tag{46}$$

starting from initial conditions at $t = 0$. For example, when the outward momentum in both pipes is the same, we have $w^-(0) = 0$. The variables w_1, w_2 in the right hand side of (44), (45) are available from w^+, w^- by

$$\begin{pmatrix} w_1 \\ w_2 \end{pmatrix} = \frac{1}{m_1 + m_2} \begin{pmatrix} m_2 & 1 \\ m_1 & -1 \end{pmatrix} \begin{pmatrix} w^+ \\ w^- \end{pmatrix}.$$

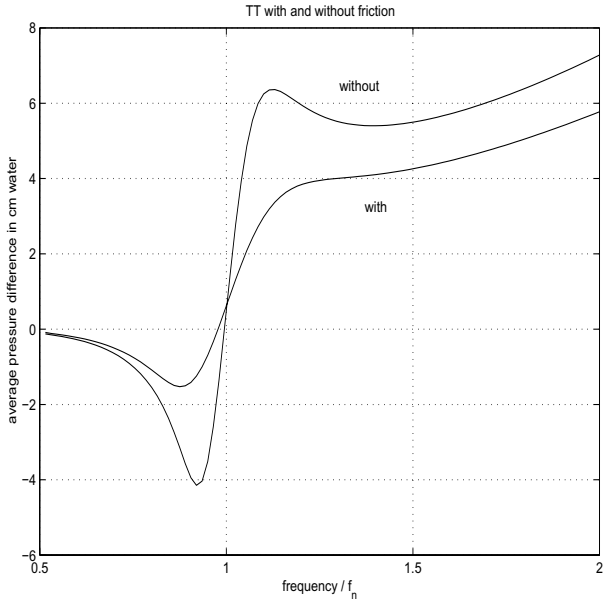

Figure 6. Average of Δp for frequencies in $[f_n/2, 2f_n]$.

For the purpose of verification we conducted simulations with (44) – (46) and computed time averages of

$$\Delta p(t) = p^a(h_2(t)) - p^a(h_1(t)) + \rho g(h_2(t) - h_1(t)),$$

the difference of the pressures at the bottom of the tanks. When the enforcement is periodic with frequency $f = \omega/2\pi$, then the trajectories are asymptotically periodic with the same frequency. Let f_n be the eigenfrequency of the linearized system, i. e. $2\pi f_n = (2q_1A_0/(m_1 + m_2)A_B))^{1/2}$. For the configuration of [11], f_n =1.368.

In Fig. 6 we plot the time averages of Δp over the ratio f/f_n for two cases: with friction as in [11] and with all friction terms set to 0, i. e. $\zeta = \zeta_{12} = p_i^v = 0$. By including one of the friction terms, we get curves in between the two of Fig. 6. Note that Fig. 6 shows time averages, while $\Delta p(t)$ itself, in the closed tanks model, oscillates between positive and negative values of magnitude roughly ten times larger than the average. We note that the curve of Fig. 6 corresponding to zero friction is very close to the curve of Fig. 8 in [11] corresponding to turbulent friction. We cannot explain this fact but as we will see, friction is not essential to have pumping in the rigid pipe models.

In the remaining of this section we consider new rigid pipe models that can be compared with the elastic tube models. A first step toward the assimilation of the configurations in [10] and [11] is to modify the model in [11] by opening up the tanks, i.e. setting $p^a = 0$. Then the eigenfrequency of the linearized system is

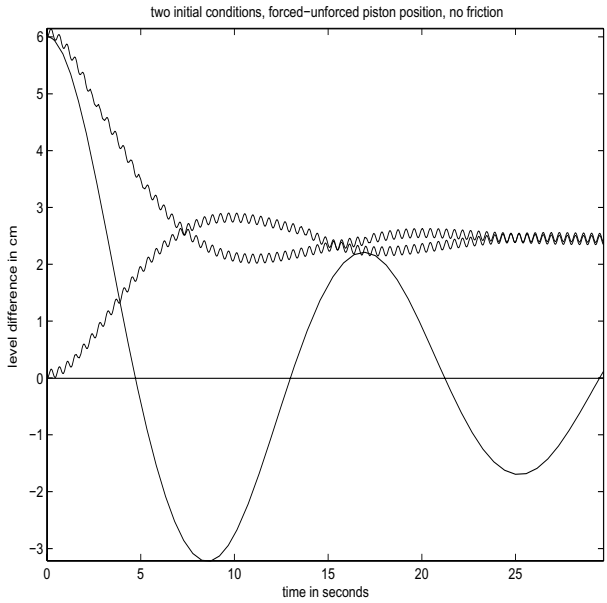

Figure 7. Response to two initial conditions with and without forcing.

$f_n = 0.07$. The average of the level difference $\Delta h = h_2 - h_1$ as a function of the frequency $f \in [f_n/2, 2f_n]$ has exactly the same form as the no-friction curve in Fig. 6, but the range of the vertical axis is reduced by a factor 400. This is due to the compression in the closed, pressurized tanks. In fact, when the enforcement is a given displacement of the piston, the level heights have the same amplitude in both models, namely 0.1 in the tank that is connected to the longer pipe of length 70, and 0.01 in the other one (pipe length 10, still using CGS-units throughout).

Numerical experiments with this model show, that the friction terms diminish the pumping effect. For example, we run simulations at the fixed forcing frequency $f = 1$ for various ratios $x_f = \ell_1/(\ell_1 + \ell_2) \in [0.05, 0.95]$. With friction terms as in [11] we see a dependence of the averaged level difference $\overline{\Delta h}(x_f)$ well approximated by $\overline{\Delta h}(x_f) = -0.4 - 13.8(x_f - \frac{1}{2})$ (thus $\overline{\Delta h}(\frac{1}{2}) = -0.4$ and $\overline{\Delta h}(0.9) \simeq -6$). With $\zeta = \zeta_{12} = p_i^v = 0$ we observe $\overline{\Delta h}(x_f) = -20(x_f - \frac{1}{2})$ (i. e. $\overline{\Delta h}(\frac{1}{2}) = 0$ and $\overline{\Delta h}(0.9) = -8$). In both cases, the averaged level is higher in the tank that is connected to the longer pipe, linearly varying with x_f .

In another set of experiments we started with various initial conditions for h_1, h_2, w^- . After a transient phase, all $\Delta h(t)$ trajectories converge to the same curve that is periodic with forcing period $1/f$ and phase according to δ . Fig. 7 shows two initial conditions ($\Delta h(0) = 0$ and $\Delta h(0) = 6$) and the model's $\Delta h(t)$ response, with ($S_p \neq 0, \delta = 0$) and without ($S_p = 0$) periodic forcing. The average $\overline{\Delta h}$ does not depend on A_B , its magnitude increases with the product

A_cS_p and decreases with d. When all parameters are fixed, the function $\overline{\Delta h}(f)$ is strictly monotone increasing for $f \geq 2f_n$; the details near $f = f_n$ aside, it is the parabola $\overline{\Delta h}(f) = 0.45f^2$. This is in contrast to the elastic tube model (cf. Fig. 3), where the pumping direction changes when f increases.

A somewhat unphysical feature of this model is the strict enforcement of the piston position, no matter how large the necessary forces are. For example, at $f = 7$, the velocity w_1 in the periodic limit oscillates between -460 and +460. At the expense of unrealistically large flow velocities, we can get arbitrarily large average level differences by increasing the product $A_cS_p\omega$. In the more moderate example of Fig. 7 the maximal asymptotic velocity is about 153 (here too $A_c = 2A, S_p = 3d/2$, but the forcing frequency is about $7/3 \simeq 38\ f_n$).

Next, we consider a third version of the model, wherein the forcing acts on the pressure above the level of the water in the cylinder at the tee. This adds degrees of freedom, since then the velocities are not as strictly coupled as above. More precisely, we consider (42), (43) with $p^a = 0, \zeta = 0$ and the following model for p_i^b: Let $p_c(t)$ be the pressure in the center at the bottom of the cylinder and assume that the velocity is zero there. Neglecting the dynamics of the fluid in the cylinder, we set

$$p_c(t) = \rho g h_0(t) + p_a(t),$$

where h_0 is the water level in the cylinder and p_a is a given forcing pressure of the form

$$p_a(t) = p_{a0} + P_a \sin(\omega t + \delta).$$

We set $p_{a0} = \rho g(\max(h_1(0), h_2(0)) - h_0(0))$. For the pressures at the entrances from the tee to the pipes we have

$$p_i^b(t) = p_c(t) - \frac{\rho}{2} w_i(t)^2. \tag{47}$$

The continuity equation now is

$$A_c \frac{d}{dt} h_0(t) = -A_0(w_1 + w_2)(t). \tag{48}$$

The rigid pipe open tanks pressure enforcement model (OTP) = [(42),(43) with $p^a = 0$, (45),(47),(48)] has the five state components w_1, w_2, h_1, h_2, h_0; a Matlab code for the computation of the right hand side of this system of ordinary differential equations is

```
function rhs = OTP(t,x)

%  rigid pipes, open tanks, pressure forcing function

w=x(1:2); h=x(3:4); h0=x(5);

global R0 dnu m rho g A0 Ac pa0 Pa omega delta A
```

```
 R = R0.*(abs(w)*dnu+eps).^(-1/4).*w.^2.*sign(w);
pe = rho*g*h - .25*rho*([1;1]-sign(w)).*w.^2;
p0 = rho*g*h0 + pa0+Pa*sin(omega*t+delta);
pb = p0 - .5*rho*w.^2;
hd = -A0/Ac*sum(w);
rhs=[(pb-pe-R)./m; A0*w./A; hd];
```

The linearization of (OTP) has two eigenfrequencies, but at neither one the pumping effect changes sign as f increases. For high frequencies and P_a fixed, $\overline{\Delta h}$ approaches zero. This seems to be physically reasonable, in contrast to the piston position model described above.

For comparison with the open tank piston position model (44) – (46) with $p^a = 0$ we tried to choose the amplitude P_a such that the asymptotic evolution of the pressure enforcement model (OTP) is similar to Fig. 7. This is the case for $P_a = 3.9p_{a0}$ (still $A_c = 2A_0$) and again the enforcement is so strong that $w_1(t)$ asymptotically oscillates between ± 148. The main new feature of this model is that the convergence to the sinusoidal limit takes longer (still all friction terms are set to 0) and at the beginning the trajectories exhibit more variation.

For comparison with the elastic tube model of section 4, note that the modelling of the forcing is different. In particular the enforcement in [10] is distributed over an extended section of the tube, whereas in the rigid pipe model the cross section of the forcing cylinder enters via the continuity equation (48) but the dynamics in the cylinder is neglected. Nevertheless, we set $A_c = d\pi(x_R - x_L)$, $\ell_1 = 54$, $\ell_2 = 126$, which are the distances of Fig. 3 from $(x_L + x_R)/2$ to the tube's ends, and use $P_a = \frac{1}{3}p_0$, which is the mean of the x-dependent amplitude in (1).

The simulation results for $\omega = 14.6$ and $\omega = 29.2$ are in Fig. 8. In contrast to Fig. 3 the asymptotic periodic limit is positive for both frequencies. For $\omega = 29.2$ it is about 4.8 (-8 in section 4). For $\omega = 14.6$ it is about 18, nine times larger than for the elastic tube model.

Attempting to find out by simulations which terms in (OTP) contribute to the pumping effect, we conducted four numerical experiments with $\ell_1 = 54$, $\ell_2 = 126$, $d = 5$, $A_c = A_0$, $P_a = p_{a0}$, $A_B = 75A_0$, $\omega = 14.6$, $\delta = 0$. First, when all friction is omitted ($p_i^v = 0$ in (42) and $\zeta = 0$ in (43)), there is more variation with the system's eigenfrequencies (see Fig. 9), and the asymptotic periodic limit of $\Delta h(t)$ is larger.

Secondly, for (OTP) with viscous friction, we looked at the effect of the terms $-\frac{1}{2}(1 - \operatorname{sign} w_i(t))\frac{\rho}{2}w_i(t)^2$ in (43). It turned out that these terms diminish the pumping effect ($\overline{\Delta h} = 0.18$ with, and $\overline{\Delta h} = 0.37$ without these terms).

Thirdly, still with nonlinear friction, we compare the case when only the $-\frac{1}{2}(1 - \operatorname{sign} w_i(t))\frac{\rho}{2}w_i(t)^2$ terms are omitted with the case when in addition the $-\frac{\rho}{2}w_i^2$ terms in (47) are omitted: In the second case $\overline{\Delta h}$ is negative, with $\Delta h(t)$ periodically being positive, see Fig. 10(a). To make $\overline{\Delta h}$ graphically visible, we used a lot of friction in the simulations for this plot.

Finally, we do the same comparison as in Fig. 10(a), but with the nonlinear

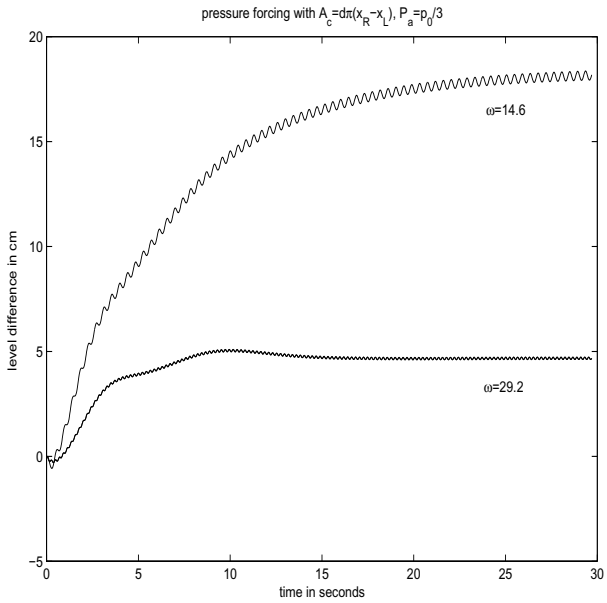

Figure 8. Comparison of the rigid pipe pressure enforcement model with the elastic tube model in Fig. 3.

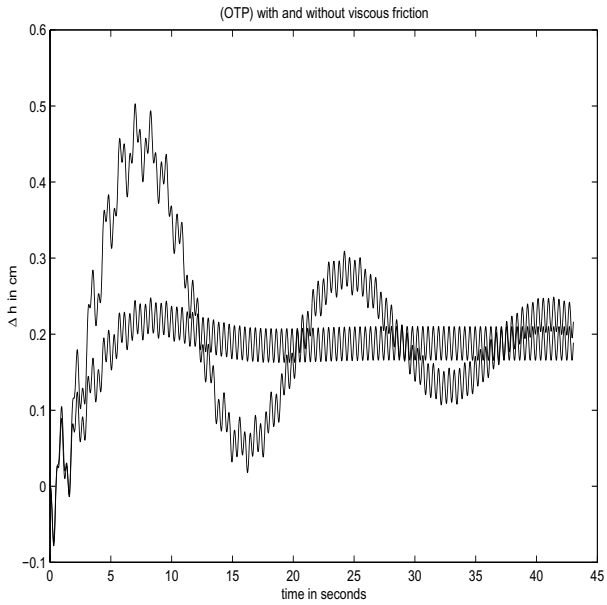

Figure 9. (OTP) with and without friction.

(turbulent) friction in p_i^v replaced by a linear (laminar) friction term as in (4), see Fig. 10(b). When all non-linearity is turned off, the average $\overline{\Delta h}$ in the rigid pipe model (OTP) is zero.

6. Conclusions

By accurate numerical simulations we clarified the controversial issue of whether or not pumping effects occur by periodic forcing in variants of an asymmetric system made of two tanks connected by an elastic tube or a rigid pipe and filled with incompressible fluid. We conclude that net pumping occurs in all variants of the model, but there are two exceptions: the linearized rigid pipe model (with linear friction) and the linearized elastic tube model without friction.

The results with the nonlinear elastic tube model showed that neither friction nor variable wave speed are essential for the pumping effect. The interplay of the wave speed and the geometry of the system was discussed. Only in the completely linearized elastic tube model, large friction is essential to produce means that are off the zero equilibrium. The (nonlinear) elasticity enhances the pumping effect, but is not strictly prerequisite. Friction diminishes the pumping effect in the nonlinear systems, but is necessary for a small average pumping effect in the linearized elastic tube model.

In the rigid pipe variant, friction terms and acceleration terms of the form $\frac{\rho}{2}w^2$ at the pipes' tank ends diminish the effect. Acceleration terms at the forcing tee increase it.

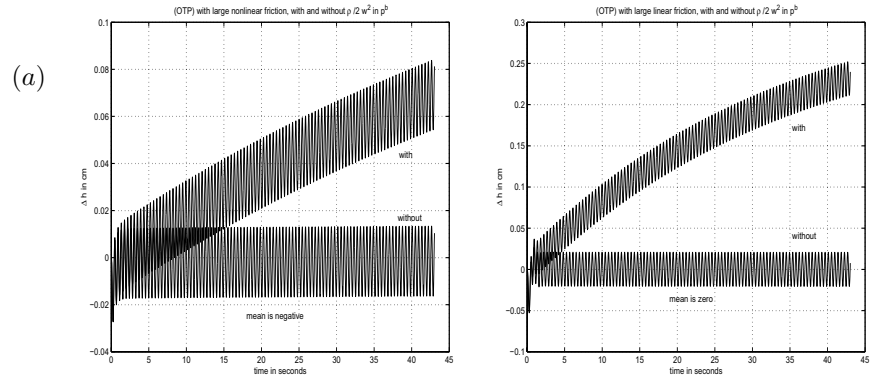

Figure 10. (a) (OTP) with and without $\frac{\rho}{2}w_i^2$ in (47); (b) (OTP) with linear friction, with and without $\frac{\rho}{2}w_i^2$ in (47).

Acknowledgement

The Liebau phenomenon and related papers were brought to our attention by D. Auerbach and T. Kenner in course of seminars of the Spezialforschungsbereich Optimierung und Kontrolle (at the Karl-Franzens-Universität and the Technische Universität in Graz, supported by grant F003 of FWF, Austria).

References

[1] H. Andersson, W. van der Wijngaart, P. Nilsson, P. Enoksson, and G. Stemme *A valve-less diffuser micropump for microfluidic analytical systems*, The MicroTAS 2000 symposium (μ TAS 2000), May 14-18, Enschede, The Netherlands.

[2] H.J. von Bredow, *Untersuchung eines ventillosen Pumpprinzips*, Fortschr. Ber. VDI-Zeitschr. Reihe 7, Nr. 9 (1968).

[3] E. Jung, *2-D Simulations of valveless pumping using the Immersed Boundary Method*, Ph.D. Thesis, Courant Institute of Mathematical Sciences, New York University (1998).

[4] D.F. Griffiths, A.M. Stuart and H.C. Yee, Numerical Wave Propagation in an Advection Equation with a Nonlinear Source Term, *SIAM J. Numer. Anal.* **29** (1992), 1244–1260.

[5] A. Harten, ENO Schemes with Subcell Resolution, *Journal of Computational Physics* **83** (1989), 148–184.

[6] A. Harten, B. Engquist, S. Osher and S.R. Chakravarthy, Uniformly High Order Accurate Essentially Non-oscillatory Schemes, III, *Journal of Computational Physics* **71** (1987), 231–303.

[7] G. Liebau, Über ein ventilloses Pumpprinzip, *Naturwissenschaften* **41** (1954), 327.

[8] M. Moser, J.W. Huang, G.S. Schwarz, T. Kenner, A. Noordergraaf, Impedance defined flow generalisation of William Harvey's concept of circulation *Int. J. of Cardiovascular Med. and Sci.* **1** (1998), 205-211.

[9] T. Naiki, M. Kawaguchi and T. Karino, Development of Valveless Pulsatile Flow Blood Pump, *Trans. Jpn. Soc. Mechanical Engineers C* **63** (1997), 680-685 (in Japanese).

[10] H.J. Rath and I. Teipel, Der Fördereffekt in ventillosen, elastischen Leitungen, *ZAMP* **29** (1978), 123–133.

[11] S. Takagi and K. Takahashi, Study of a Piston Pump without Valves, *Bulletin of JSME* **28** (1985), 831–836.

[12] D. Tomanek and R.J. Enbody (Eds.), *Science and Application of Nanotubes*, Kluwer Academic/Plenum Publishers, New York, 2000.

[13] E.F. Toro, *Riemann Solvers and Numerical Methods for Fluid Dynamics*, Springer-Verlag, Berlin, 1997.

Alfio Borzì
Institut für Mathematik
Karl-Franzens-Universität Graz
Heinrichstr. 36
A-8010 Graz
Austria
e-mail: alfio.borzi@uni-graz.at

Georg Propst
Institut für Mathematik
Karl-Franzens-Universität Graz
Heinrichstr. 36
A-8010 Graz
Austria
e-mail: georg.propst@uni-graz.at

(Received: September 12, 2001)